

Dynamics of circular arrangements of vorticity in two dimensions

Rohith V. Swaminathan¹, S. Ravichandran², Prasad Perlekar², and Rama Govindarajan² †

¹ MIT/WHOI Joint Program in Oceanography, Massachusetts Institute of Technology, Cambridge, MA 02139, USA

² TIFR Centre for Interdisciplinary Sciences, Tata Institute of Fundamental Research, Hyderabad 500075, India

(Received ?; revised ?; accepted ?. - To be entered by editorial office)

The merger of two like-signed vortices is a well-studied problem, but in a turbulent flow, we may often have more than two like-signed vortices interacting. We study the merger of three or more identical co-rotating vortices initially arranged on the vertices of a regular polygon. At low to moderate Reynolds numbers, we find an additional stage in the merger process, absent in the merger of two vortices, where an annular vortical structure is formed and is long-lived. Vortex merger is slowed down significantly due to this. Such annular vortices are known at far higher Reynolds numbers in studies of tropical cyclones, which have been noticed to break down into individual vortices. In the pre-annular stage, vortical structures in a viscous flow tilt and realign in a manner similar to the inviscid case, but the pronounced filaments visible in the latter are practically absent in the former. Five or fewer vortices initially elongate radially, and then reorient their long axis closer to the azimuthal direction so as to form an annulus. With six or more vortices, the initial alignment is already azimuthal. At higher Reynolds numbers, the merger of an odd number of vortices proceeds very differently from that of an even number. The former process is rapid and chaotic whereas the latter proceeds more slowly via pairing events.

The annular vortex takes the form of a generalised Lamb-Oseen vortex (GLO), and diffuses inwards until it forms a standard Lamb-Oseen vortex. For lower Reynolds number, the numerical (fully nonlinear) evolution of the GLO vortex follows exactly the analytical evolution until merger. At higher Reynolds numbers, the annulus goes through instabilities whose nonlinear stages show a pronounced difference between even and odd mode disturbances. Here again, the odd mode causes an early collapse of the annulus via decaying turbulence into a single central vortex, whereas the even mode disturbance causes a more orderly progression into a single vortex. Results from linear stability analysis agree with the nonlinear simulations, and predict the frequencies of the most unstable modes better than they predict the growth rates.

It is hoped that the present findings will motivate studies on how multiple vortex interactions affect the inverse cascade in two-dimensional turbulence.

1. Introduction

Vortices may be considered to be fundamental building blocks of turbulent flows. Merger events are believed to be of central importance in the inverse cascade of turbulent kinetic energy in two-dimensional turbulence (???). In a turbulent flow dense

† Email address for correspondence: rama@tifrh.res.in

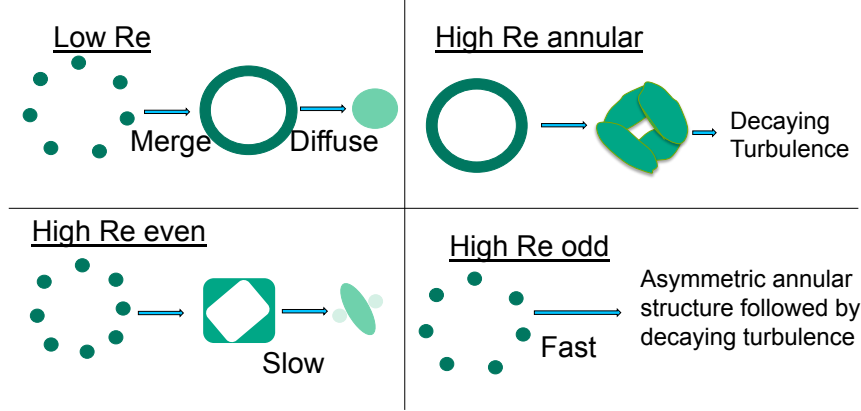


FIGURE 1. A schematic summarizing the dynamics. At low Reynolds number, n co-rotating vortices will merge to form an annular structure, which then diffuses inwards to form a single Lamb-Oseen vortex. At high Reynolds number, an annular vortex is not stable. It breaks into several vortices, and creates decaying turbulence. n vortices at high Reynolds number will form an annulus-like structure which is symmetric when n is even and asymmetric when n is odd. The former will decay into a tripolar structure while the latter will break down quickly into decaying turbulence.

with vorticity, the most common form of interaction is between two vortices, but it is not unusual for three or more vortices to interact. While the merger process of two identical vortices is extremely well-studied (see e.g. ??), the simultaneous interaction in viscous flow of three or more vortices has not been studied in the context of merger, to the best of our knowledge. In this paper, we investigate the merger and breakup of several vortices and the breakup of an annulus of vortex.

We study a model flow consisting of several (upto 9) equal like-signed vortices placed initially on the vertices of regular polygons, and find that the merger of $N > 2$ vortices shows several features distinct from the two-vortex case. The summary of our findings is depicted schematically in fig. 1. Vortex merger depends on both whether the number of vortices is odd or even, and on the Reynolds number of the flow. At relatively low Reynolds number, we find an annular vortex stage in the merger process. This annular structure remains axisymmetric but reduces in radius to eventually produce a single merged Lamb-Oseen vortex. On the other hand the evolution at high Reynolds numbers is more complicated. An annular vortex loses symmetry and the flow becomes turbulent as it decays. The vortices in a system of an even number of vortices, e.g. 6 or 8, pair up to form a 4 vortex configuration which then undergoes further mergers. More fascinating is the case of merger of an odd number of vortices. Here, all vortices cannot pair and the merger process is more turbulent. The system rapidly degenerates into decaying turbulence.

We also numerically investigate the stability of an annular vortex. This problem was first studied by ?, who performed inviscid stability analysis and numerical simulations with broadband initial perturbations and found a ring of elevated vorticity perturbed with azimuthally broad-banded initial conditions to go unstable and form multiple vortices, which undergo further rearrangement to a near monopolar circular vortex. We study how the wavenumber of the initial perturbation affects the stability of the annular vortex, and find similar growth rates for the $m = 4$ mode as Schubert *et al.*.

At low Reynolds number the annular vortex is stable and its amplitude decays via

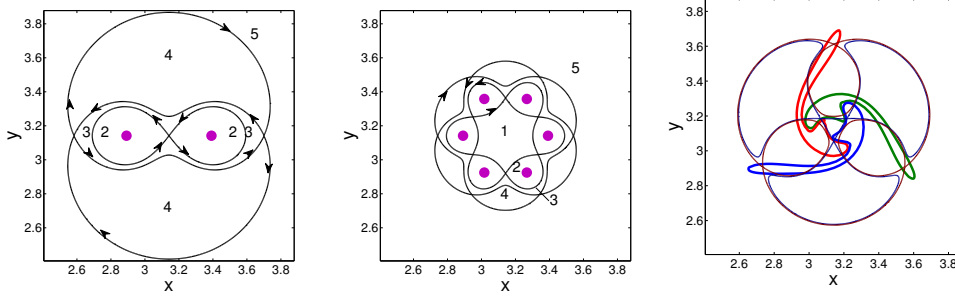


FIGURE 2. Separating streamlines in the co-rotating frame for (a) two and (b) six point vortices. The vortices are indicated by large (pink online) dots. The regions are distinguished as follows: (1) central (not present for 2 vortices), (2) inner core, (3) exchange band, (4) outer recirculating and (5) external flow. (c) Separatrices for three point vortices (dotted lines) overlaid on three patches of uniform vorticity in inviscid evolution (solid lines).

diffusion. However at higher Reynolds number the annular vortex becomes unstable. The linear growth rate is positive for a range of azimuthal wavenumber, and the variation with wavenumber is smooth. In the nonlinear stages of disturbance growth, however, we see some interesting behavior. Similar to vortex merger at high Reynolds number, the nonlinear destabilisation of the annular vortex strongly depends on whether the initial perturbation is even or odd. This final stage of the merger process is the similar to what happens in inviscid flow, where a thin annulus often goes unstable and bunches up into several patches of vorticity.

We first examine what is known about the inviscid case because it provides a comparison and contrast with the viscous study to follow.

2. Dynamics of multiple vortices in inviscid flow

Consider an inviscid system with n co-rotating point vortices, each of circulation Γ/n , and separated by a distance $d/2$ from the centroid of the system, as shown in figure 2. These vortices are confined by the Biot-Savart law to motion on a circle of diameter d , with an azimuthal velocity of $u_\theta = (n-1)\Gamma/(n\pi d)$. In a coordinate frame rotating with the same angular velocity as the vortices, the system is in steady state, with the positions of the vortices, as well as the streamlines, frozen. There are several saddle points in this frame of reference, and the vortices themselves act as centers. Streamlines connecting the saddle points, either homoclinically or heteroclinically, form separatrices in the flow, as shown in figures 2(a) and (b) for two and six vortices respectively. The separatrices divide the fluid flow into distinct regions: (1) central, (2) inner core, (3) exchange band, (4) outer recirculating and (5) external flow. In regions 2 and 4, flow follows closed streamlines in the rotating coordinate system, so the fixed points within these are centers. The outer recirculating region has fluid rotating in a sense opposite to the inner core and exchange band regions. Only region 2 contains vorticity. The central region exists only when we have three or more vortices, this is evident in figures 2 (b) and (c). The exchange band is well-known in the two-vortex viscous case to be of importance during the merger process, we will see how it affects the dynamics in the multiple vortex case.

The point vortex system was shown long ago (??) to be unstable for $n > 7$. Among the host of studies that followed, we pick our way through only the most relevant for the present work. Primary among these is ? who extended the work of Thomson to the case of n finite patches of uniform vorticity rather than point vortices, placed initially at the

vertices of a regular polygon, and allowed to undergo inviscid dynamics. If the vortices have finite but small radius a , such that (a/d) is much less than a critical ratio $(a/d)_{crit}$, the dynamics is similar to that of point vortices. Larger inviscid patches do not remain circular but their shapes may be obtained exactly. If $(a/d) \geq (a/d)_{crit}$, the vortices, while rotating around each other, deform and also move towards each other, but Kelvin's circulation theorem prevents any reconnection of their boundaries. In the case of vortices with finite size, non-linear inviscid studies (?) so far have indicated that these vortices collapse into an annulus-like structure. A typical placement and shape of patch vortices in this process is superimposed on the separatrices in figure 2(c). The inviscid simulations have been carried out using a contour dynamics code from ?. In the inviscid case too, a significant departure from periodic motion on a circle will occur only if $(a/d)_i \geq (a/d)_{crit}$. We therefore begin these simulations with $(a/d)_i = 0.26$. The initial convective stage is seen to be similar in the inviscid and viscous cases. However, the realignment and shape are different at later stages, and sharper filaments of exchange-band vorticity are seen. When the patches are too close or the filaments too thin, inviscid simulations cannot continue.

An inviscid annular vortex on the other hand goes unstable to azimuthal disturbances and splits into smaller multiple vortices ?. Symmetric neutral disturbances of large azimuthal wavenumber are the only ones that resist instability.

3. Simulations of vortex merger

3.1. Numerical scheme and initial conditions

Since the flow is incompressible and two-dimensional, we may work with the vorticity and streamfunction equations:

$$\left(\frac{\partial}{\partial t} + \frac{\partial \psi}{\partial y} \frac{\partial \omega}{\partial x} - \frac{\partial \psi}{\partial x} \frac{\partial \omega}{\partial y} \right) \omega = \nu \nabla^2 \omega, \quad (3.1)$$

$$\nabla^2 \psi = -\omega, \quad (3.2)$$

where ω and ψ are the vorticity and streamfunction respectively, x and y are spatial coordinates and t is time. We solve this system by a Fourier pseudo-spectral technique (??) for spatial discretization, with a standard de-aliasing by zero padding using the 3/2 rule. Simulations at high Reynolds numbers and those for the stability of an annular vortex structure are time evolved with an exponential Adams-Bashforth temporal discretization. Unless stated otherwise, we work with a square domain of area $4\pi^2$ and discretize it with N^2 collocation points with $N = 2048$.

At the initial time, n identical co-rotating vortices (n varying from 2 to 8) are arranged at equal intervals on the circumference of a circle of radius R i.e. on the vertices of a regular polygon. Each of these vortices has a gaussian initial vorticity profile given by $\omega = \omega_0 e^{-r^2/a^2}$, with a total circulation in the system given by Γ . Here r is the radial location measured from the centre of each vortex. In all our simulations, we prescribe $(a/d)_i = 0.1$ at $t = 0$, where the subscript i refers to initial conditions. To make fair comparisons between cases of different n , we follow two approaches. In the first case, we keep the total initial circulation Γ constant across the set of simulations. The Reynolds number is then given by

$$Re_\Gamma = \frac{\Gamma}{\nu}, \quad (3.3)$$

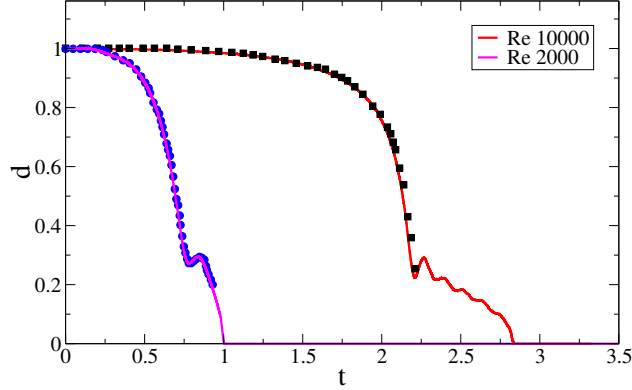


FIGURE 3. Evolution of the separation distance in the merger of two identical vortices. The results of ? ($Re = 2000$) and ? ($Re = 10000$) compared to present simulations.

and the time scale is the period of rotation of point vortices of the same strength, given by

$$T_{\Gamma} = \frac{2n\pi^2 d^2}{(n-1)\Gamma}. \quad (3.4)$$

In the following, wherever we refer to Re without a subscript, we mean Re_{Γ} .

In the second case, we keep the total initial energy, within a domain of diameter d_0 , constant across the set of simulations. The Reynolds number is based on the root mean square velocity u_{rms} within this domain, and its size:

$$Re_E = \frac{u_{rms} d_0}{\nu}, \quad (3.5)$$

with the time scale $T_E = d_0/u_{rms}$.

All the results presented here use an initial separation $d_i = 0.5$ for the vortices.

In viscous flow, two vortices which come close enough to touch each other merge into one vortex. This process has been described in great detail, see e.g., [1]. If the initial radius of each vortex is much smaller than the distance separating their centers, the vortices rotate at a constant frequency as described above. Simultaneously they grow in size by viscous diffusion. Once their radius reaches a critical fraction ($= 0.22$) of their separation distance, enough vorticity has entrained into the exchange band, which creates filamentary structures that induce a radially inward velocity on the vortices, bringing them close to each other. This is followed by a second diffusive stage where the separation decreases slowly to 0, whence an axisymmetrization of the merged vortex follows. The filamentary debris is erased by viscosity during this time. A typical history of the separation distance is shown in figure 3 which also serves as a validation of our numerical approach.

To contrast later with multiple-vortex merger, we present in fig. 4 the viscous evolution of two gaussian vortices. Notice the tilt of the vortices with respect to the radial coordinate at intermediate times, and the filaments in the outer region.

3.2. Merger of multiple vortices at moderate Reynolds number

To show why three or more vortices are different from two, we return to Fig. 2. The annular nature of the exchange band region and the consequent existence of a central passive region means that for $n \geq 3$ vortices tend to align azimuthally rather than radially. The formation of an azimuthally restrained vortical structure is evident in figure 2(c).

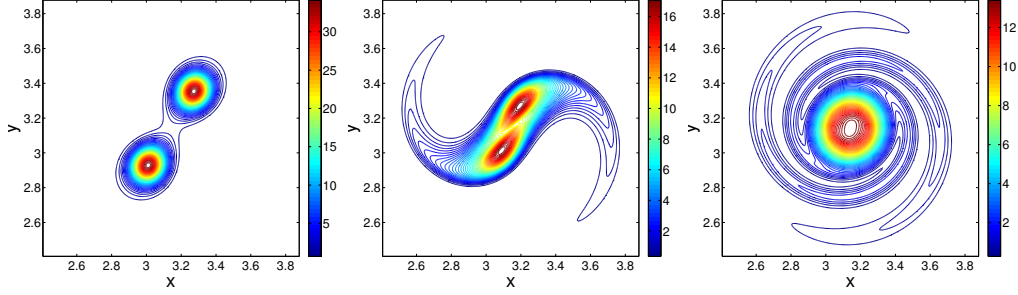


FIGURE 4. Viscous evolution of two gaussian vortices with $(a/d)_i = 0.1$ and $Re_\Gamma = 4000$. (a) $t=0.669$ (b) $t=1.52$ (c) $t=2$.

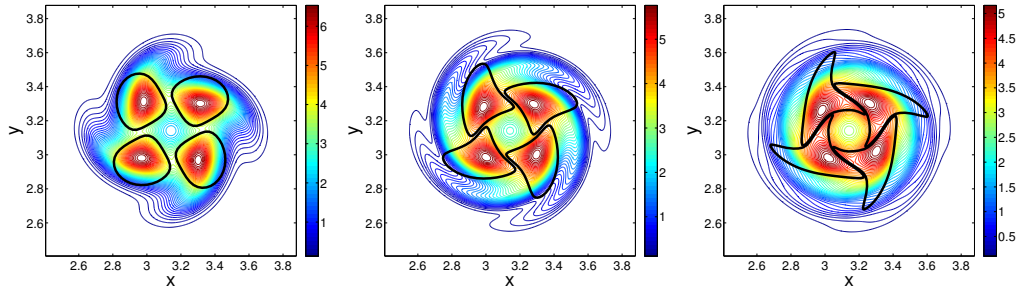


FIGURE 5. Viscous evolution of four gaussian vortices with $(a/d)_i = 0.3$ and $Re_\Gamma = 4000$. A gentle initial radial alignment is seen. (a) $t=0.81$ (b) $t=2.43$ and (c) $t=4.86$. The solid black lines show the inviscid evolution of patch vortices at the corresponding times.

Such a structure will be contrasted with an axisymmetric annulus formed in viscous merger.

Four-vortex merger is shown in Fig. 5. The inviscid and viscous dynamics are similar at early times. The central region is seen to be affecting the dynamics, effecting an azimuthal realignment, and in the viscous case, giving rise at later times to an axisymmetric annular structure (not shown). The case of three vortices is not shown for brevity, but it proceeds in a manner very familiar to the four vortex case. Fig. 6 shows the viscous evolution of six gaussian vortices. The strain field now is such that even at short times, the vortices align themselves azimuthally, forming an axisymmetric annulus. Note that such axisymmetry is impossible in inviscid evolution. There is then a slow reduction in radius of the annulus on a diffusive time scale, to finally form a single gaussian vortex. The formation of filaments is minimal, unlike in the merger of two vortices. To summarize, merger is now an azimuthal phenomenon, like people on a dance floor joining hands to form a circle, and does not result immediately in the formation of a vorticity maximum at the centre. The latter is attained on a diffusive time scale.

Fig. 7(a) shows the distance d of the maximum vorticity point of each vortex from the centre, as a function of time t , for different number of vortices, at $Re_\Gamma = 4000$. The length and time are non-dimensionalised respectively by the initial separation d_i and the time scale T_Γ . A bend in the curve, where the coming together of the vortices slows down, is evident at $n = 3$ and $n = 4$. This bend corresponds to the formation of the annulus. Consequently, the convective stage is shorter in these cases. The convective stage completely disappears for six or more vortices. We have instead a new annular stage which is diffusive. Thus, the annular stage dominates the merger process as we increase

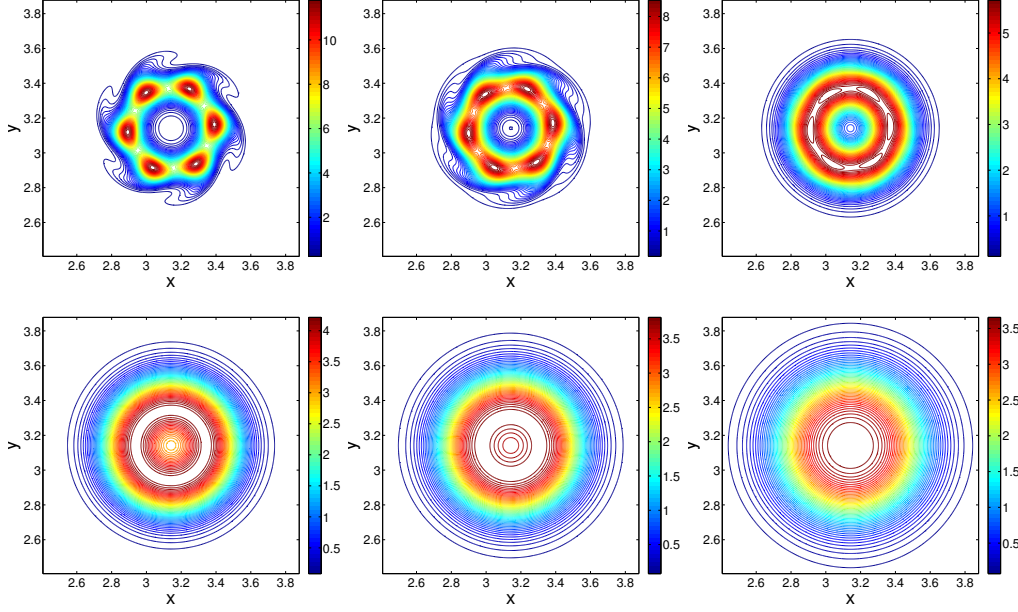


FIGURE 6. Viscous evolution of 6 gaussian vortices with $(a/d)_i = 0.1$ and $Re_\Gamma = 4000$. Observe initial azimuthal alignment, very clean annulus, and the subsequent inward motion of the annulus to form a single maximum. (a) $t=1$ (b) $t=1.52$ (c) $t=2.7$ (d) $t=5.4$ (e) $t=7.5$ (f) $t=10.47$.

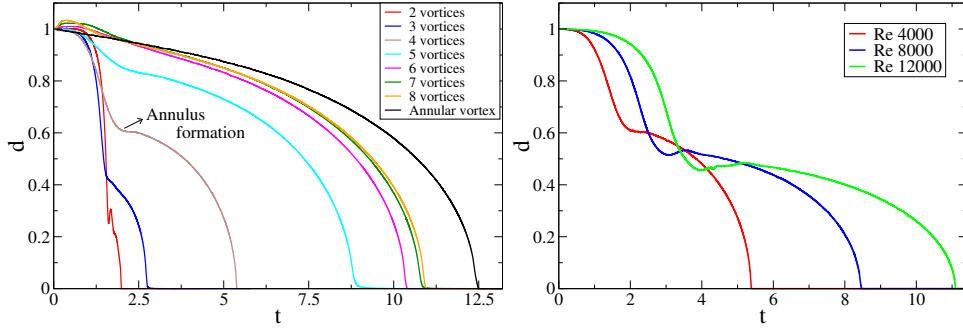


FIGURE 7. (a) Non-dimensional separation distance d (scaled by the initial separation) as a function of the non-dimensional time t at $Re_\Gamma = 4000$. Starting with six or more vortices is qualitatively the same as starting with a pure annular vortex. Here $(a/d)_i = 0.1$. (b) Separation distance d versus time t for four vortices, for different Re_Γ .

the number of vortices, and spans the entire merger process for six and more vortices. This is a slow stage and effectively delays the merger. It can also be seen that as we increase the number of vortices, the process ceases to depend on the number of vortices. As we increase the number of vortices, there is a reduction in filament formation, which helps to slow down the approach of the vortices towards each other. In the simulations above, we have kept the initial Γ the same as we increase the number of vortices, and one may argue that in order to make a fair comparison between two different systems, it is the initial energy which has to be kept the same and not the initial circulation. We repeated all these simulations keeping the initial energy the same as we changed n , and we found that nothing changes qualitatively. The annular stage once again increasingly dominates the merger process as n increases, and effectively delays the merger.

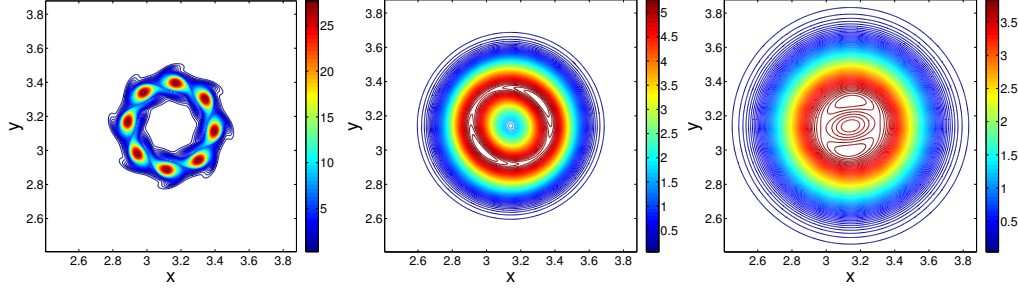


FIGURE 8. Viscous evolution of 8 gaussian vortices with $(a/d)_i = 0.1$ and $Re_\Gamma = 12000$. (a) $t=0.1685$ (b) $t=10.0447$ (c) $t=25.0276$.

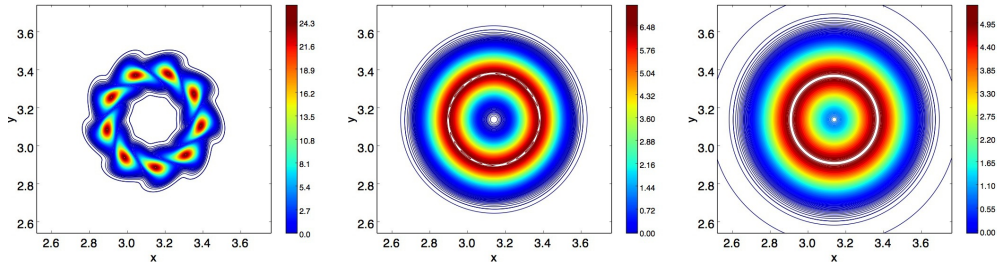


FIGURE 9. Viscous evolution of nine gaussian vortices with $(a/d)_i = 0.1$ and $Re_\Gamma = 12000$ at times (in units of T_Γ): $t = 0.09$ (left panel) , $t = 4.59$ (middle panel) , and $t = 9.09$ (right panel).

Next we study the effect of changing Re_Γ on four vortex merger, this is shown in Fig. 7(b). As expected, the duration of the first diffusive stage increases as the Reynolds increases. This is because the critical (a/d) is reached at a later time for lower relative viscosity. As is also true of the two-vortex case, the convective stage is almost independent of the Reynolds number. Most important, the final (annular) stage of merger is strongly dependent on the Reynolds number, with the duration scaling approximately linearly with the Reynolds number, suggesting that the annular stage is a diffusive stage.

We now look at what happens with eight and nine vortices. We choose $Re_\Gamma = 12000$ and $(a/d)_i = 0.1$. The results are shown in Fig. 8 for 8 vortices and Fig. 9 for 9 vortices. In both cases, the merger proceeds as discussed before in that the annulus forms and migrates inwards, but in the eight vortex case, a small departure from axisymmetry, in the form of a tripolar vortex, is visible at late times. In the next section, we will contrast these results against eight and nine vortex dynamics at very high Reynolds number.

3.3. High Reynolds number multiple vortex simulations

At higher Reynolds number, nonlinearity dictates the dynamics and the viscosity is not effective in making the vortices diffuse and merge. To capture the small scale structures that appear at high Reynolds number, we discretised the computational domain with 4096^2 collocation grid points. We find that the dynamics strongly depends on whether the number of vortices are even or odd (a feature not observed in linear stability).

3.3.1. Six-vortex merger, $Re_\Gamma = 1.5 \times 10^5$

We begin with an even number (six) of vortices arranged, as before, on the vertices of a regular polygon. The plot in Fig. 10 shows the time evolution of the vorticity contours during the merger process. Initially, the dynamics proceeds in a manner similar to that at

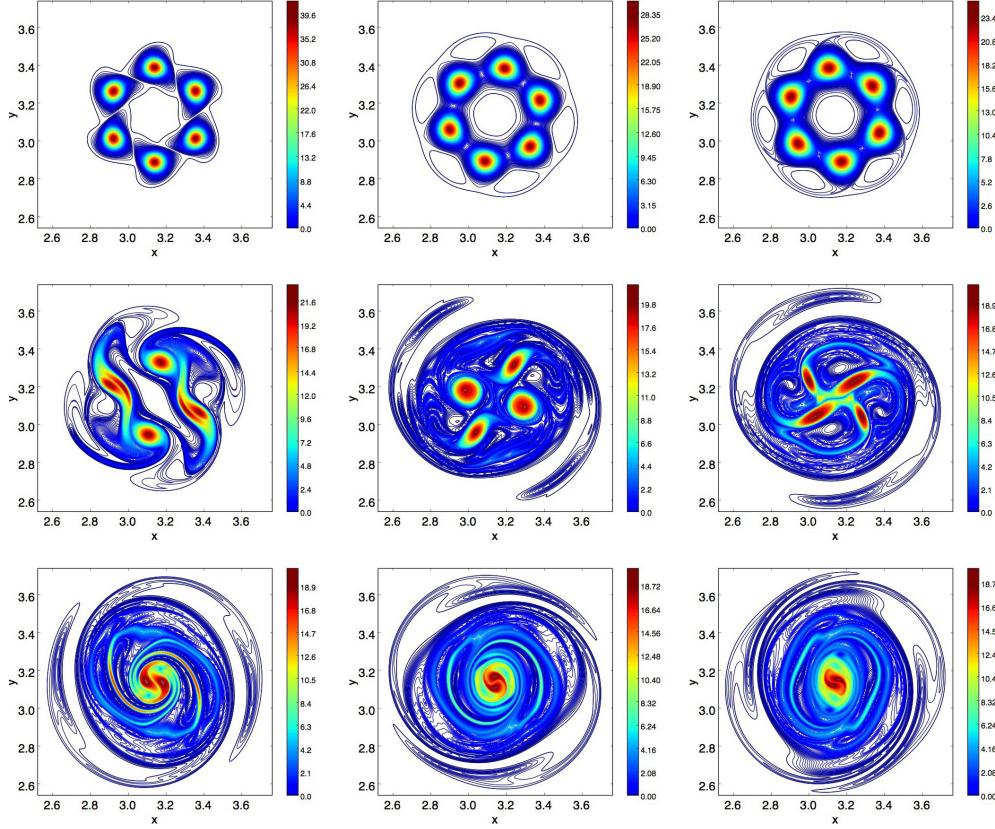


FIGURE 10. Contours of vorticity showing the time evolution of a 6 vortex configuration at $Re_\Gamma = 1.5 \cdot 10^5$. The different snapshots are at times (in units of $T_\Gamma \approx 0.74$) $t = 0.09$ (top-left), $t = 6.42$ (top-center), $t = 10.64$ (top-right), $t = 12.75$ (middle-left), $t = 14.86$ (middle-center), $t = 15.71$ (middle-right), $t = 16.13$ (bottom-left), and $t = 16.55$ (bottom-center), and $t = 16.89$ (bottom-right).

moderate Reynolds number. The vortices start to rotate in the counterclockwise direction and try to form an annular like structure. The annulus, however, is never formed. The six vortices undergo an asymmetric merger to first form four vortices, which are not identical. The two located diametrically opposite to each other, which came from the merger events are larger. This is followed by another pair of mergers to give two vortices, with a lot of fine filamentary structure in the neighbourhood.

3.3.2. Eight-vortex merger, $Re_\Gamma = 2 \times 10^5$

We now examine a multiple of four (i.e. eight) vortices on the vertices of a regular polygon, in Fig. 11. Now the first merger event is perfectly symmetric, with four pairwise mergers yielding four identical vortices. The eight-vortices pair-wise merge event to form four vortices that are surrounded by thin filamentary structures. The perfect symmetry of this case is preserved through most of the later dynamics, whereas this is not possible in the six and nine vortex cases. Here the four vortex structure continues to decay until, at a later stage, these vortices further merge to form a tripolar vortex.

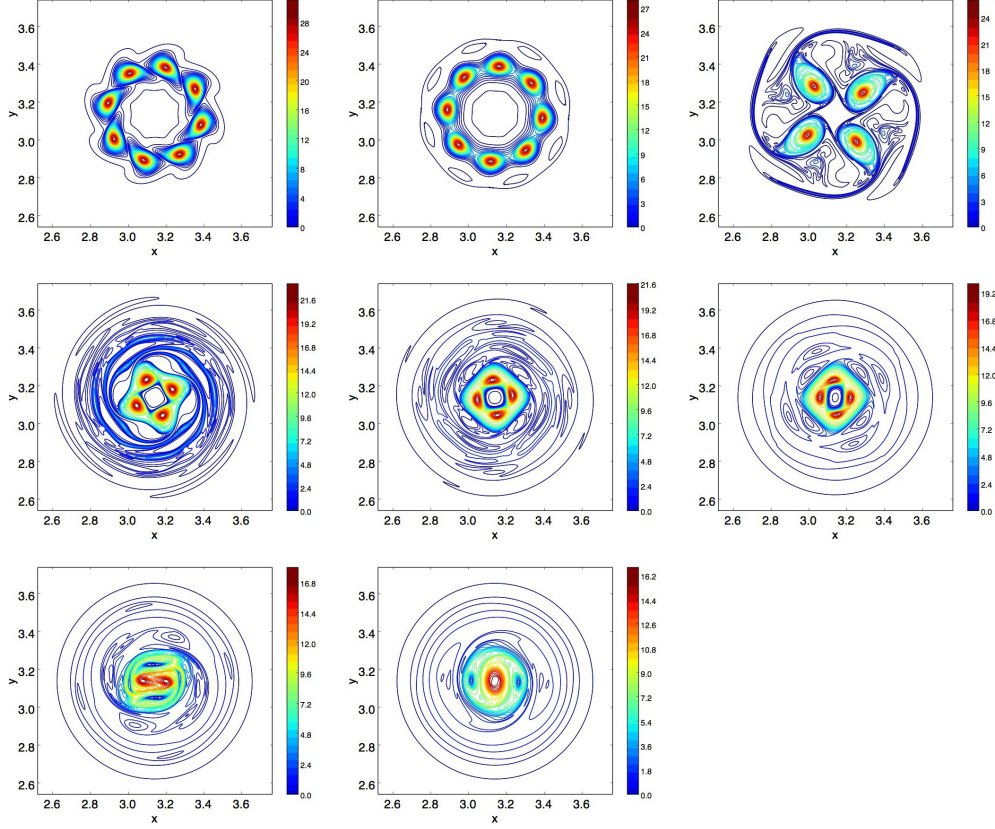


FIGURE 11. Contours of vorticity showing the time evolution of an 8 vortex configuration at $Re_\Gamma = 2 \cdot 10^5$. The different snapshots are at times (in units of T_Γ) $t = 0.09$ (top-left), $t = 2.31$ (top-center), $t = 4.52$ (top-right), $t = 6.74$ (middle-left), $t = 8.96$ (middle-center), $t = 11.17$ (middle-right), $t = 13.39$ (bottom-left), and $t = 15.60$ (bottom-right).

3.3.3. Nine-vortex merger, $Re_\Gamma = 2 \times 10^5$

The dynamics of an odd number (nine) of vortices arranged initially on the vertices of a regular polygon is very different from its even-number counterpart. The plot in Fig. 12 shows the time evolution of the vorticity contours during the merger process. Initially the vortices start to rotate in the counter-clockwise direction and form an annular structure. However, because of an additional unpaired vortex this structure very quickly turns unstable and chaotic. We point out that, because of rapid mixing, the total time of merger is about half what is expected. At late times a single vortex at the centre of the domain is formed.

4. The generalized Lamb-Oseen vortex

We have seen that at moderate Reynolds numbers an annular vortex is formed. This vortex can be written down analytically as an exact solution of the axisymmetric Navier-Stokes equations. The analytical solution for the annular vortical structure from the viscous evolution of a circular vortex sheet was derived by ?. We provide an alternative derivation in the appendix. We call this solution the generalized Lamb-Oseen (GLO) vortex with vorticity concentrated within an annulus. Such a vortex results from the

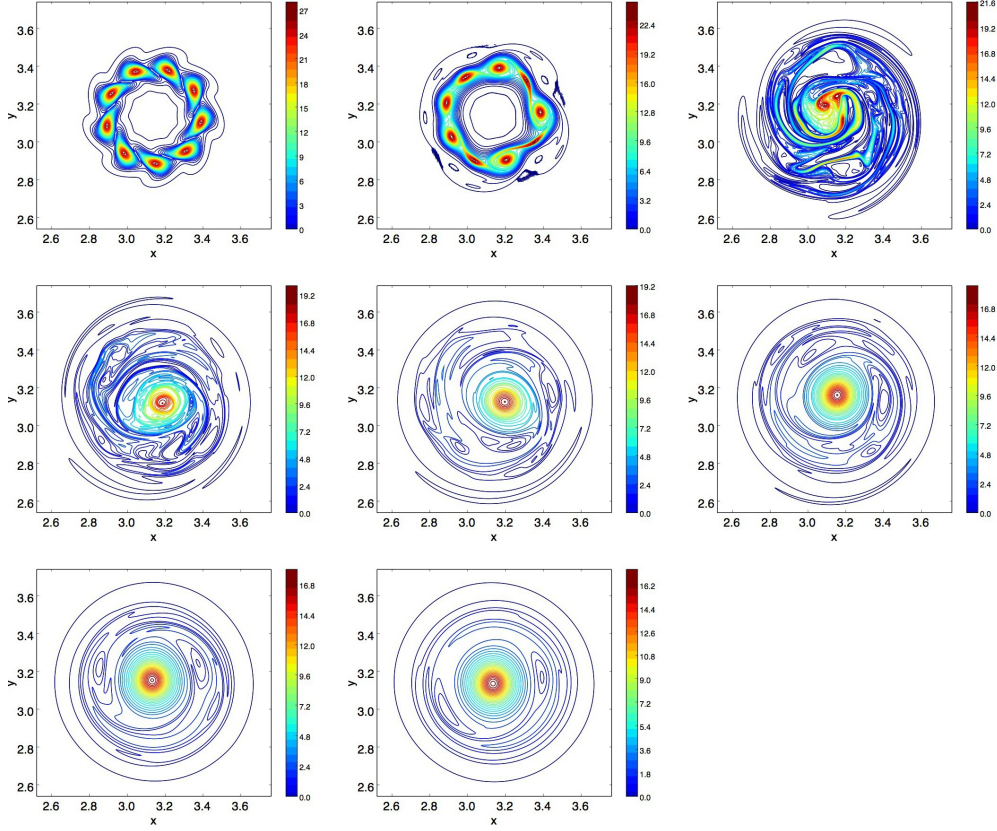


FIGURE 12. Contours of vorticity showing the time evolution of a nine vortex configuration at $Re_\Gamma = 2 \cdot 10^5$. The different snapshots are at times (in units of T_Γ) $t = 0.09$ (top-left), $t = 2.34$ (top-center), $t = 4.59$ (top-right), $t = 6.85$ (middle-left), $t = 9.09$ (middle-center), $t = 11.35$ (middle-right), $t = 13.59$ (bottom-left), and $t = 15.85$ (bottom-right).

evolution of a cylindrical vortex sheet at a radius a with a circulation of Γ_o , given at $t = 0$ by

$$\omega(r, 0) = \frac{\Gamma_o}{2\pi r} \delta(r - a), \quad (4.1)$$

by the axisymmetric vorticity equation

$$\frac{\partial \omega}{\partial t} = \frac{\nu}{r} \frac{\partial}{\partial r} \left(r \frac{\partial \omega}{\partial r} \right). \quad (4.2)$$

The boundary conditions are symmetry at $r = 0$ and a vorticity-free far-field. The generalized Lamb-Oseen vortex (see Appendix) is then obtained as

$$\omega = \frac{\Gamma_o}{4\pi\nu t} e^{-\left(\frac{a^2 + r^2}{4\nu t}\right)} I_0\left\{\frac{ar}{2\nu t}\right\}, \quad (4.3)$$

where I_0 is the modified Bessel function of the first kind and zeroth order. Setting a to zero reduces the above to a standard Lamb-Oseen vortex. It is useful to note the non-dimensional parameter $\nu t/a^2 = b^2$, which controls the profile of the GLO. Further, it is interesting to note that differentiating Eq. 4.3 with respect to time will yield additional solutions which satisfy the Navier-Stokes, including some that have net zero circulation.

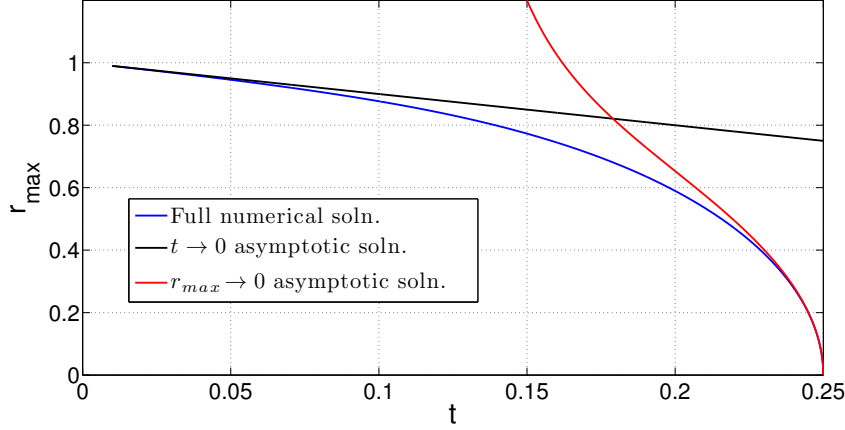


FIGURE 13. Location of vorticity maximum r_{max} . Time is non-dimensionalised by a^2/ν .

At $t \rightarrow 0$, we may write the vorticity and, with some algebra, the location r_{max} of the vorticity maximum, at leading order in t as

$$\omega = \frac{\Gamma_o}{4\pi^{3/2}a\sqrt{\nu t}} \exp\left[-\frac{(r-a)^2}{4\nu t}\right], \quad r_{max} = a - \frac{1}{a}\nu t, \quad t \rightarrow 0. \quad (4.4)$$

Thus the vorticity maximum will move inwards purely due to diffusion, initially in a ballistic manner. Next, we may estimate the behavior as $r_{max} \rightarrow 0$ by writing, at leading order,

$$r_{max} = \frac{4\sqrt{2}\nu t}{a} \sqrt{\frac{a^2 - 4\nu t}{8\nu t - a^2}}. \quad (4.5)$$

The time taken for the vorticity maximum to reach the center is thus $a^2/(4\nu)$. Thus, for $\nu t/a^2 = b^2 < 0.25$, the GLO is an annular vortex sheet with the vorticity maxima away from the axis. For such a profile, a smaller b^2 corresponds to a thinner annular sheet. However, for $b^2 \geq 0.25$, we obtain a vortex with a vorticity maximum at the axis. Fig. 13 contains plots for the evolution of r_{max} and its early and late behavior, given by equations 4.4 and 4.5.

In our simulations of merger above, in the cases when an annular vortex was arrived at, we found that the annular structure was, to a good approximation, the GLO vortex. In the following section we begin with a GLO vortex and perform numerical simulations with the method described above to check the analytical solution against the dynamics obtained numerically, and to study the stability of the annular structure.

4.1. Direct Numerical Simulations of the Generalised Lamb Oseen vortex

The linear and nonlinear stability of annular vortices has been well studied under the inviscid framework. ? considered an annular Rankine vortex with a fixed outer radius and variable inner radius, and showed it to linearly unstable when the inner radius exceeds half the outer radius. The cases which are linearly stable go through a steepening and sharpening of disturbance waves when nonlinearity is included, but reach a stable state nevertheless. The nonlinear instability leads to a breaking up into multiple vortices, an example of a five vortex steady state emerging from an instability of the annular vortex is demonstrated.

The existing literature contains studies that report annular vortices becoming unstable

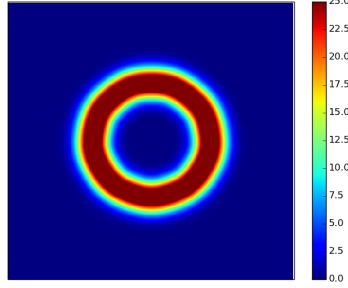


FIGURE 14. Initial GLO vortex. The dark red regions indicate regions of intense vorticity whereas the blue regions indicate regions of low vorticity. In all figures showing vorticity contours in the rest of the paper we have used the same colorbar.

to several modes of imposed perturbations. ? report that initially thin annular vortices breakup in an $m = 5$ mode, and initially thick annular vortices break up in an $m = 3$ mode, forming mesovortices. ? study the stability of an annular vortex under imposed $m = 2$ perturbations and find that wave-interactions may damp the growth of the perturbations. ? find the existence of $m = 3$ and $m = 4$ modes in an actual Hurricane.

We conduct a series of direct numerical simulations of the two-dimensional Navier-Stokes (NS) equations to study the evolution of the GLO vortex, and its stability to small perturbations of odd and even azimuthal wavenumber m . In what follows, the Reynolds number $Re_\Gamma \equiv \Gamma/\nu$ was varied by reducing the viscosity ν and keeping the circulation Γ fixed at a value of 6. To generate the GLO, we set the parameter $\nu_t \equiv \nu t = 0.001$, the distance from origin $a = 0.25$, and fix (π, π) as the centre. The vertical y and horizontal x distances are measured from this centre. We prescribe different values for the initial perturbation ϵ (see the remainder of section 4 and section 5). Radial perturbations are added by modifying the radius of a given vorticity to $r \rightarrow r + \epsilon \sin[m \tan^{-1}(y/x)]$, where m defines the azimuthal wavenumber of the perturbation. The initial vortex structure for a GLO with a small perturbation is shown in Fig. 14. As it is unrealistic to scan the whole (m, Re_Γ) phase-space with numerical simulations, we choose a few representative Reynolds numbers for four modes of disturbance, the even modes $m = 4$ and $m = 8$ and the odd modes $m = 5$ and $m = 9$.

At a Reynolds number of 30000 we compare, in figure 15, numerical simulations of the dynamics of an annular vortex against the predicted evolution of the GLO from equation (4.3). These simulations were done with $\epsilon = 0.001$. In this case, the perturbations do not grow visibly so we expect a good comparison with the theoretical GLO. The initial vortex in both is the same, and the width δ of the annular vortex in both cases is measured between the radial locations at which the vorticity drops to $1/e$ of its maximum value. Note that there are no fitting parameters. The widening with time of the annular region, as well as corresponding reduction in maximum vorticity of the numerical solution agrees extremely well with the theoretical GLO. In the radial location of the maximum vorticity, the agreement between theory and simulations is very good at early times, but a departure from GLO behavior is seen at later times. The reason for this small departure could be small growths in the initial perturbations.

We next present, in figure 16, how the width of the annular vortex varies with time at a given azimuthal angle at a Reynolds number of 45000, for an $m = 4$ perturbation of amplitude 10^{-6} of the reference vorticity. At this Reynolds number, oscillations in the width are evident at moderate times. The axisymmetric analytical solution is shown for

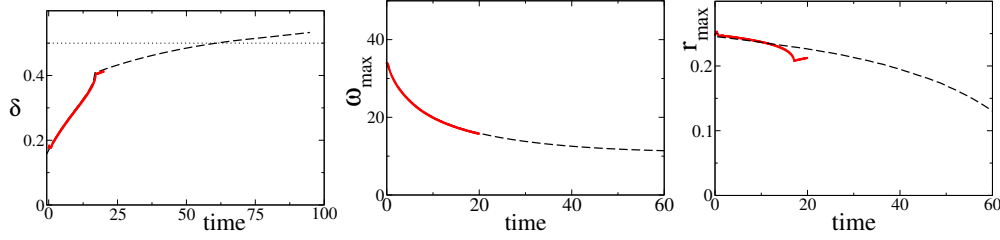


FIGURE 15. Comparison of analytical evolution of the generalized Lamb-Oseen vortex with direct numerical simulations for $Re = 30000$. (a) Width of the annular region. (b) Maximum vorticity. (c) Location of the vorticity maximum. The black dashed lines are from the analytical expression whereas the solid red line is from the simulations.

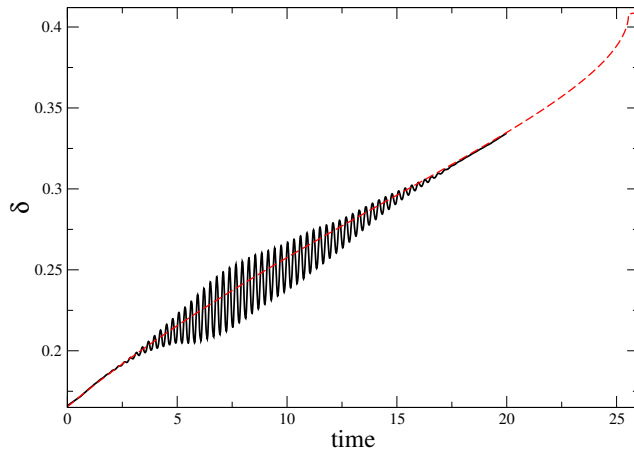


FIGURE 16. Variation of the width of an annular vortex of $Re = 45000$ with time (solid black line). The initial condition contains an $m = 4$ perturbation of amplitude 10^{-6} of the reference vorticity. The analytical GLO evolution is shown by the red dashed line.

comparison and is seen to be a good indicator of the growing width of the annular region. These oscillations grow for some time, and then decay.

Like the multiple-vortex systems above that behave differently for odd and even numbers of vortices, the annular vortex responds differently to perturbations of odd and even azimuthal wavenumbers. We now discuss some cases to illustrate this.

4.1.1. Even mode radial perturbations: $m = 8$

The plot in Fig. 17 shows the evolution of a GLO vortex with an $m = 8$ mode perturbation. For Reynolds numbers $Re \leq 4.5 \cdot 10^4$, the vortex ring is stable to initial perturbations. On increasing the Reynolds number beyond $Re_{\Gamma} = 90000$ we observe that an initial instability sets in that makes a “4 vortex necklace” like structure. A similar structure had been seen in the early simulations of ? (who used $Re = 10^5$ and an azimuthally broadband initial perturbation). For $Re = 9 \cdot 10^4$ the vortex necklace disappears at intermediate times, but another instability seems to appear at late times. On the other hand, for $Re \geq 1.35 \cdot 10^5$ the vortex necklace breaks into a tripolar vortex. Figure 18 shows the evolution of the width at a particular azimuthal angle of the annulus for $Re = 45000$ and perturbations of azimuthal wavenumber $m = 8$. It is seen that high frequency oscillations occur at early times, which decay and give rise to low frequency oscillations at later times. The initial oscillations correspond to an $m = 8$ mode, as prescribed, whereas the low frequency oscillations are of $m = 4$, as is evident in Fig. 17

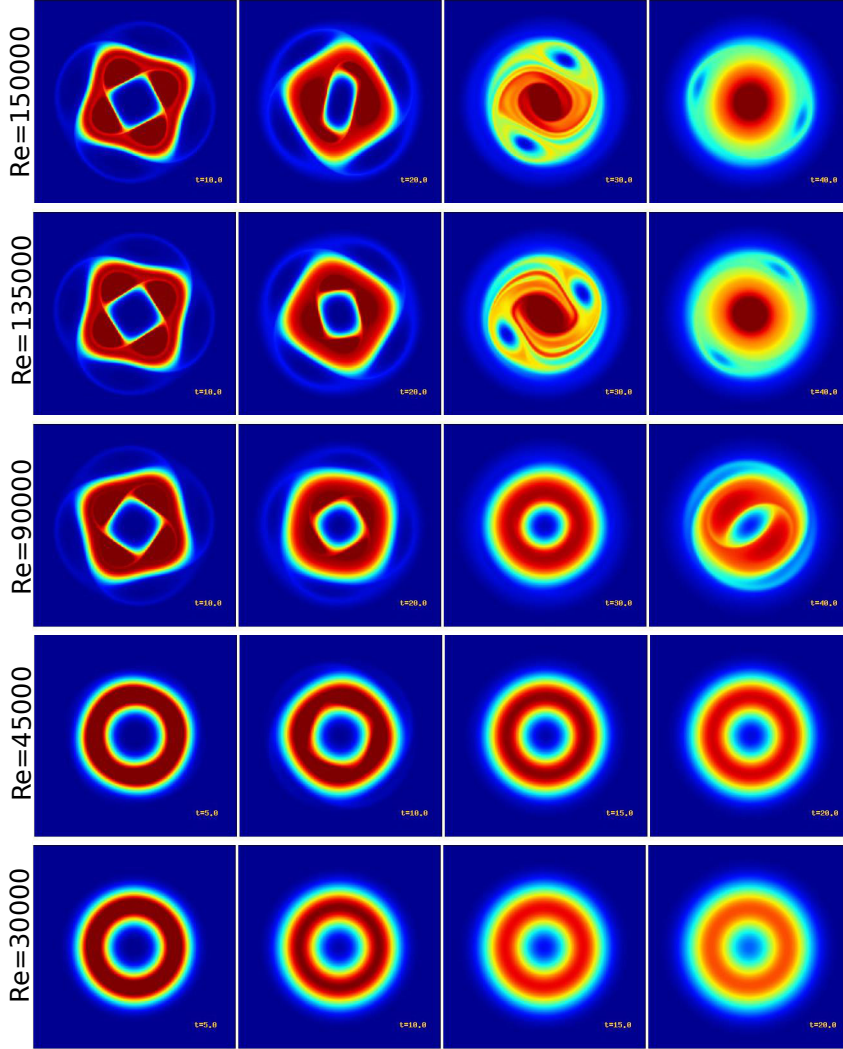


FIGURE 17. Time evolution of the GLO annular vortex with an $m = 8$ mode perturbation for various Reynolds number. For small Reynolds number the GLO is stable and the radial perturbations decay. At $Re = 9 \cdot 10^4$ instabilities start to appear. For even larger Reynolds numbers $Re = [1.35, 1.5] \cdot 10^5$, the GLO breaks into a 4 vortex structure that later evolves into a tripolar vortex structure.

for this Reynolds number at a time of 10. Our provision of an $m = 8$ perturbation thus facilitates the growth of $m = 4$ perturbations. These in turn die down at this Reynolds number, as was seen in Fig. 17 at later times, and viscous processes take over.

4.1.2. Odd mode radial perturbation: $m = 5$ and 9

The plots in Figs. 19 and 20 show the time evolution of a GLO vortex with $m = 5$ and $m = 9$ mode perturbations at different Reynolds number. At $Re = 30000$ and above, the $m = 9$ mode is linearly stable (see section 5), but triggers the $m = 4$ mode which is unstable. We therefore see a 4-vortex necklace. The $m = 5$ mode is linearly unstable above $Re = 30000$ and becomes turbulent without forming the 4-vortex necklace.

A striking feature is that even the qualitative nature of evolution of instabilities is

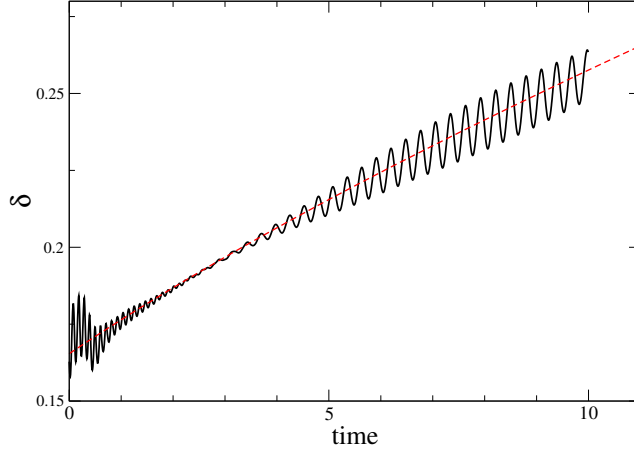


FIGURE 18. Time variation of the width of an annular vortex at $Re = 45000$ with an initial $m = 8$ perturbation. Oscillations of this azimuthal wavenumber are seen at early times, which die down and give way to $m = 4$ perturbations visible at later times. As before the dashed line is the analytical GLO evolution.

different for odd and even mode perturbations. For small values of Reynolds number the vortex ring is stable to odd-mode perturbations, as to even mode. On increasing the Reynolds number beyond $Re = 90000$, we do observe, with odd mode perturbations too, that an initial instability sets in that makes a “4 vortex necklace” like structure. At a later stage however, in contrast to the $m = 8$ mode perturbation, this structure breaks into filamentary structures and forms a turbulent patch. This feature stems from the fact that the vortex necklace is now less symmetric.

We next perform a linear stability analysis of the annular GLO vortex in order to better understand the results from our nonlinear simulations. We do not, however, expect the linear stability analysis to capture subtle differences between odd and even perturbation wavenumbers.

5. Linear stability analysis of an annular vortex

A thin cylindrical vortex sheet is linearly stable to axisymmetric perturbations in inviscid flow, as given by the condition for inviscid stability of ?, that $(rV)^2$ (V being the swirl velocity), should nowhere decrease as the radius r increases. ? found such a vortex sheet to be unstable to non-axisymmetric perturbations ($m \geq 1$, where m is the azimuthal wave number), so while Rayleigh’s criterion is necessary and sufficient for axisymmetric disturbances, for non-axisymmetric disturbances it is necessary but not sufficient. ????? have studied different aspects of inviscid stability in two and three dimensions, and it is evident that a cylindrical vortex is inviscidly unstable to non-axisymmetric perturbations. There are also several inviscid stability studies in the context of hurricanes and tornadoes. ? report that their inviscid stability calculations show a maximum growth rate for the $m = 4$ mode. No studies, to our knowledge, have addressed the question of what happens in the viscous case, and so we conduct a viscous linear stability analysis.

The present problem is a time-varying one, and a linear stability study can only be conducted by making the frozen flow approximation. We use as our base flow a vorticity profile frozen at a given instant of time. This quasi-steady approximation is the time-analog of a parallel flow approximation made for spatially developing flows. The GLO vortex produces an entirely axisymmetric flow in which the nonlinear terms vanish. Per-

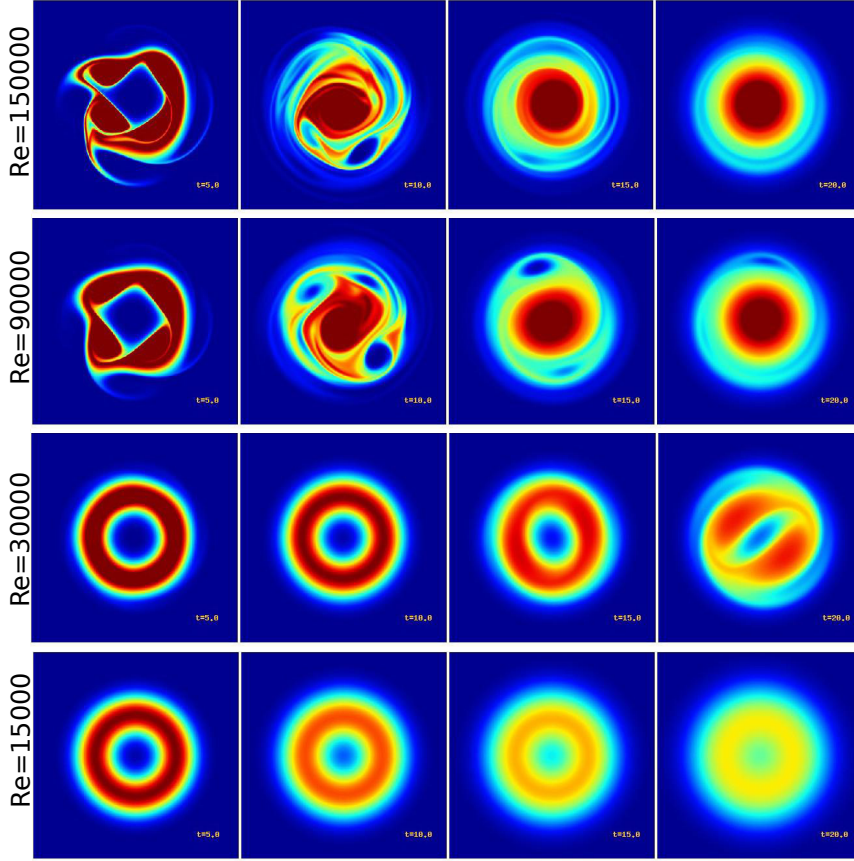


FIGURE 19. Time evolution of the GLO annular vortex with an $m = 5$ mode perturbation for various Reynolds number. For small Reynolds number the GLO is stable and the radial perturbations decay. However, at larger Reynolds number the GLO breaks into a 4 vortex necklace. On further increasing the Reynolds number, this structure breaks up into a turbulent patch.

turbations imposed on the axisymmetric initial state bring the nonlinear terms into play. As the GLO vortex gets smoothed out by viscosity, we expect that the flow becomes less unstable to perturbations.

Following the standard procedure, we decompose the total motion into a background state and express the perturbations in their normal mode form, characterized by an azimuthal wavenumber m and a complex frequency f , as, e.g. for the azimuthal component of velocity

$$u_{\theta_{tot}} = U_{\theta}(r) + \hat{u}_{\theta}(r) e^{i(m\theta - ft)}. \quad (5.1)$$

Substituting such expressions into the two-dimensional incompressible continuity and Navier-Stokes equations in plane polar co-ordinates, neglecting nonlinear terms in the perturbations, and eliminating pressure and \hat{u}_{θ} , we are left with an eigenvalue problem in the radial velocity component u_r :

$$A\hat{u}_r = fB\hat{u}_r. \quad (5.2)$$

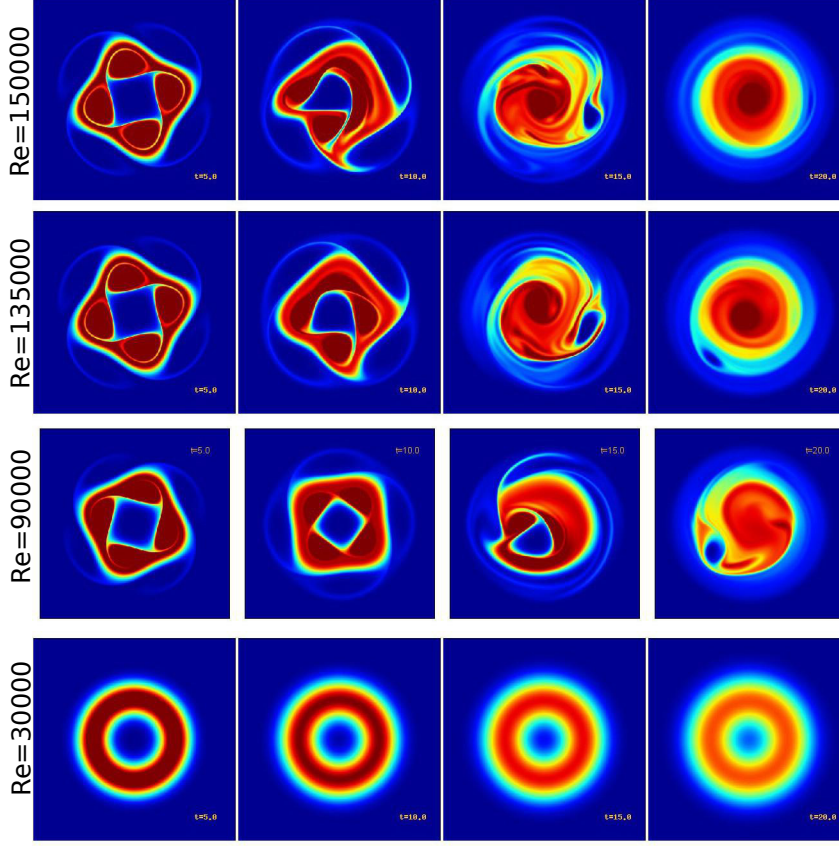


FIGURE 20. Time evolution of the GLO annular vortex with an $m = 9$ mode perturbation for various Reynolds number. For small Reynolds number the GLO is stable and the radial perturbations decay. However, at larger Reynolds number the GLO breaks into a 4 vortex necklace. On further increasing the Reynolds number, this structure breaks up into a turbulent patch.

The system is stable if the imaginary part of f , i.e., $f_i < 0$ and unstable if $f_i > 0$. A and B are linear differential operators given by

$$A = i\nu \left\{ r^2 D^4 + 6rD^3 + (5 - 2m^2) D^2 - \frac{(1 + 2m^2) D}{r} + \frac{(m^2 - 1)^2}{r^2} \right\} + m\Omega \{ r^2 D^2 + 3rD + (1 - m^2) \} - mrZ', \quad (5.3)$$

and

$$B = \{ r^2 D^2 + 3rD + (1 - m^2) \}, \quad (5.4)$$

where $D \equiv d/dr$, angular velocity $\Omega = U_\theta/r$, and base flow vorticity $Z = U'_\theta + U_\theta/r$. Primes denote derivate with respect to r . The linear stability equations (5.2, 5.3, 5.4) are the same as equation (3.1) in ?, written for constant density. The boundary conditions depend on the mean profiles, which obey $U_\theta \sim r$ as $r \rightarrow 0$, $U_\theta \sim 1/r$ as $r \rightarrow \infty$. The boundary conditions are then deduced from the leading order terms of the Taylor series

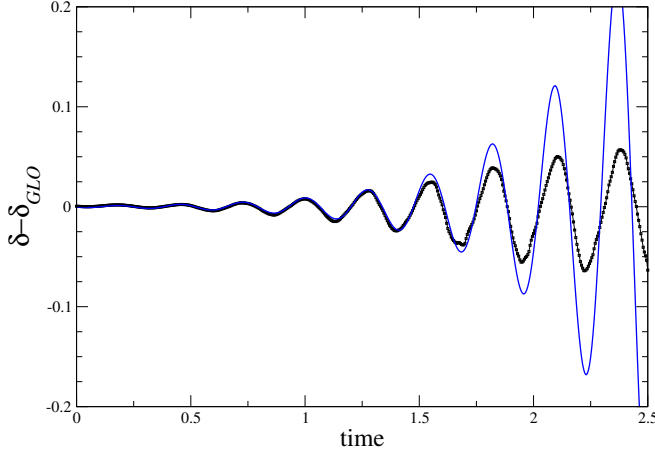


FIGURE 21. A best fit of the oscillations seen at moderate times. Symbols: numerical simulations at $Re = 45000$, with an $m = 4$ perturbations of amplitude 10^{-3} in the vorticity. The line is a fit, given by equation (5.7).

about $r = 0$ and $r \rightarrow \infty$, satisfying, for large Reynolds numbers,

$$\hat{u}_r \sim r^{|m|-1}, \text{ for } r \rightarrow 0, \quad \text{and } \hat{u}_r \sim r^{-|m|-1} \text{ as } r \rightarrow \infty. \quad (5.5)$$

A similar exercise for three-dimensional perturbations yields exponential, rather than algebraic, decay at large r . These boundary conditions were originally derived by ? in the form of compatibility relations, and were formalized later on by ? and ?.

We study the linear stability of the GLO vortex of equation (4.3). We have made detailed comparisons with a smoothed annular Rankine profile and get no qualitative difference in the answers. We solve the eigenvalue problem above using a Chebyshev collocation technique. To specify a grid in the domain $[0, R_{max}]$, and to cluster grid points into the vicinity of the annular vortex, we use a modified version of the algebraic stretching used by ?, given by

$$y = \frac{x(1 - \xi^3)}{q_1 + q_2\xi + (1 - q_2)\xi^3}, \quad q_1 = 1 + \frac{2x}{R_{max}}, \quad x = \frac{pR_{max}}{R_{max} - 2p}, \quad (5.6)$$

where ξ is the Chebyshev coordinate lying in $[-1, 1]$, p is the radius at which clustering is required, and q_2 is chosen to lie between 0.5 and 0.8. We have also used the exponential stretching of ? and obtained the same answers. Our computational domain extends up to $R_{max} = 1000$, and with the number of Chebychev collocation points N of up to 1000.

Instability growth rates, as well as the azimuthal wavenumbers, increase with increasing Reynolds number and, at high Reynolds numbers, are very similar to inviscid predictions. We discuss linear stability results for a Reynolds number of 45000, which is high enough that disturbance growth is visible to the naked eye in the simulations, and small enough that at long times, viscous effects take over and the annulus returns to a GLO vortex. The circular frequency and growth rate of the most unstable perturbations from linear stability predictions, in the non dimensional units of the simulation, are given in figure 22.

Figure 22 also shows the existence of two $m = 2$ modes that are unstable. The slower-growing of the two is the same as that of ?. A more detailed analysis of the faster growing $m = 2$ mode will be done elsewhere, but since this is not the most unstable mode, it is not discussed further in the present study.

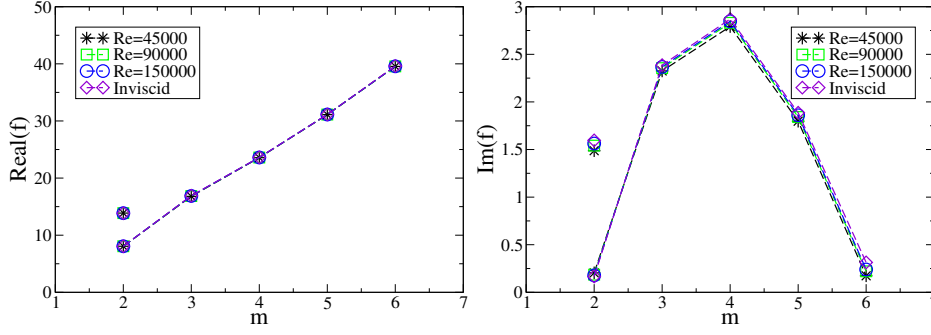


FIGURE 22. Circular frequency (left) and growth rate (right) as a function of azimuthal wavenumber from the linear stability analysis. The $m = 4$ mode has the highest growth rate, and there are two unstable $m = 2$ modes (see text).

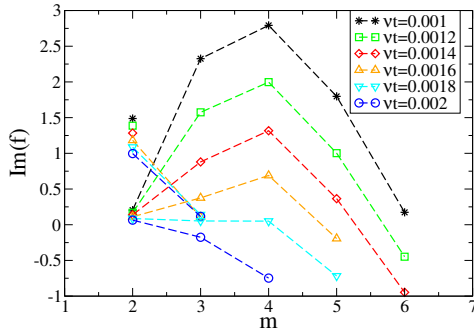


FIGURE 23. Growth rate (right) as a function of azimuthal wavenumber for varying initial δ or $b^2 = \nu t/a^2$ from the linear stability analysis for a Reynolds number of 45000. $\nu t = 0.001$ corresponds to our initial profile or a simulation time of zero. $\nu t = 0.002$ corresponds to a simulation time of 7.5.

To compare the linear stability results with nonlinear dynamics, we return to the oscillations seen in figure 16. We subtract the width of the GLO vortex at every time, and plot the oscillations at early times in figure 21. Shown in the same figure is a best-fit curve, given by

$$\delta - \delta_{GLO} = 0.0008e^{2.5t} \sin[23t - 2.5]. \quad (5.7)$$

It is seen that the frequency of the oscillation is close to the value of 23.6 predicted by linear theory for $m = 4$. This frequency is maintained constant over a long time. However, we do not see any reasonable stretch of exponential growth, so nonlinearities are important throughout the evolution. We have performed $m = 4$ simulations with three amplitudes of initial perturbation, 10^{-6} , 10^{-3} and 10^{-2} . All three show oscillations whose frequency is extremely well fitted by a value of 23. Exponential growth only occurs over short stretches of time in each case, and these best-fit growth rates are different, at 1.75, 2.5 and 3.5 respectively. These growth rates compare well with the linear stability growth rate of 2.8. The simulation of ? was for a Reynolds number of 10^5 , and although they used only 512^2 grid points at this high Reynolds number, the growth rate they report is also comparable. In the figure 18, we find initial oscillations of azimuthal wavenumber 8 whose frequency is very close to the value of 58.17 obtained by linear stability, but no evidence of exponential growth. The $m = 4$ oscillations at later time are of frequency close to 24. Such behaviour is not uncommon in shear flows, with the frequency predicted

by linear stability studies being quite prominent in the dynamics even after nonlinearities have become dominant.

6. Conclusions

To summarise, we have shown that $n \geq 3$ identical vortices placed at the vertices of a regular polygon tend, at moderate Reynolds number, to align themselves into a long-lived annular structure. The annular vortex may be described analytically as a generalised Lamb Oseen vortex, which diffuses slowly inwards to form a single gaussian vortex at long times. The annular stage dominates the merger process more as the number of vortices increases, effectively delaying the merger. At high Reynolds numbers, a single vortex at the centre is attained at large times, but there is no annular structure formation. Remarkably, and the behaviour for odd and even number of vortices is qualitatively different. When n is even, the merger process at high Reynolds numbers is characterised by vortex pairing events rather than annulus formation. The option of complete vortex pairing is not available when n is odd, and a breakdown into chaotic motion is seen. In a much shorter time than when n is even, a single central vortex is formed.

We then study the annular vortex in some detail, performing numerical simulations and (viscous) stability analysis. The time evolution of our numerical simulations of the annular vortex agrees extremely well with our generalised Lamb Oseen solution for low Reynolds numbers. Our numerical simulations show that the annular vortex is stable to imposed perturbations at $Re = 45000$ and below, while instabilities clearly influence dynamics at $Re = 90000$ and above. The nonlinear evolution of even and odd mode perturbations is strikingly different. Again the odd mode perturbations result in a more chaotic flow, and collapse to a single vortex at much shorter times, whereas even modes proceed via reduction of wavenumber to effect a large slow down of the inverse cascade process.

This work, we hope, will motivate experimenters and simulators of two-dimensional turbulence to evaluate the contributions to the inverse cascade of multiple vortex interactions.

Appendix

Taking the Laplace transform in time of Eqs. 4.2 and using Eq. 4.1, we get

$$\frac{d^2 \hat{\omega}}{dr^2} + \frac{1}{r} \frac{d\hat{\omega}}{dr} - \frac{s\hat{\omega}}{\nu} = -\frac{\omega(r, 0)}{\nu} = f(r), \quad (6.1)$$

where $\hat{\omega}$ is the Laplace transform of ω . The homogeneous part is a modified Bessel equation in the variable $r\sqrt{\frac{s}{\nu}}$, whose solution is

$$\hat{\omega}_h = c_1 I_0 \left(r\sqrt{\frac{s}{\nu}} \right) + c_2 K_0 \left(r\sqrt{\frac{s}{\nu}} \right), \quad (6.2)$$

where I_0 and K_0 are modified Bessels functions of the first and second kind respectively (?). The particular solution is obtained by variation of parameters, as

$$\hat{\omega}_p = I_0 \left(r\sqrt{\frac{s}{\nu}} \right) \int_0^r r' f(r') K_0 \left(r'\sqrt{\frac{s}{\nu}} \right) dr' - K_0 \left(r\sqrt{\frac{s}{\nu}} \right) \int_0^r r' f(r') I_0 \left(r'\sqrt{\frac{s}{\nu}} \right) dr', \quad (6.3)$$

The complete solution $\hat{\omega} = \hat{\omega}_h + \hat{\omega}_p$. Applying the boundary conditions, which require that $\hat{\omega}$ be finite at $r = 0$, and that $\hat{\omega} \rightarrow 0$ as $r \rightarrow \infty$, and remembering that K_0 and I_0

diverge respectively as $r \rightarrow 0$ and ∞ , we get

$$\hat{\omega} = \begin{cases} \frac{\Gamma_o}{2\pi\nu} I_0 \left(r \sqrt{\frac{s}{\nu}} \right) K_0 \left(a \sqrt{\frac{s}{\nu}} \right) & \text{for } r \leq a , \\ \frac{\Gamma_o}{2\pi\nu} I_0 \left(a \sqrt{\frac{s}{\nu}} \right) K_0 \left(r \sqrt{\frac{s}{\nu}} \right) & \text{for } r > a . \end{cases} \quad (6.4)$$

It can be seen that the symmetry condition (Eq. 6.1) is automatically satisfied. Taking the inverse Laplace transform, and using the following standard result from ?,

$$L^{-1} \left\{ K_n \left[\sqrt{s} \left(\sqrt{\alpha} + \sqrt{\beta} \right) \right] I_n \left[\sqrt{s} \left(\sqrt{\alpha} - \sqrt{\beta} \right) \right] \right\} = \frac{1}{2t} e^{-\left(\frac{\alpha+\beta}{2t}\right)} I_n \left\{ \frac{\alpha + \beta}{2t} \right\} , \quad (6.5)$$

we get equation (4.3).